OPEN

Journal of Cerebral Blood Flow & Metabolism (2015) 35, 1249–1259

www.jcbfm.com

ORIGINAL ARTICLE

# Chronic cerebral hypoperfusion induces vascular plasticity and hemodynamics but also neuronal degeneration and cognitive impairment

Zhen Jing[1,6], Changzheng Shi[2,6], Lihui Zhu[3], Yonghui Xiang[3], Peihao Chen[2], Zhilin Xiong[1], Wenxian Li[1], Yiwen Ruan[3,4,5] and Li'an Huang[1]

Chronic cerebral hypoperfusion (CCH) induces cognitive impairment, but the compensative mechanism of cerebral blood flow (CBF) is not fully understood. The present study mainly investigated dynamic changes in CBF, angiogenesis, and cellular pathology in the cortex, the striatum, and the cerebellum, and also studied cognitive impairment of rats induced by bilateral common carotid artery occlusion (BCCAO). Magnetic resonance imaging (MRI) techniques, immunochemistry, and Morris water maze were employed to the study. The CBF of the cortex, striatum, and cerebellum dramatically decreased after right common carotid artery occlusion (RCCAO), and remained lower level at 2 weeks after BCCAO. It returned to the sham level from 3 to 6 weeks companied by the dilation of vertebral arteries after BCCAO. The number of microvessels declined at 2, 3, and 4 weeks but increased at 6 weeks after BCCAO. Neuronal degeneration occurred in the cortex and striatum from 2 to 6 weeks, but the number of glial cells dramatically increased at 4 weeks after BCCAO. Cognitive impairment of ischemic rats was directly related to ischemic duration. Our results suggest that CCH induces a compensative mechanism attempting to maintain optimal CBF to the brain. However, this limited compensation cannot prevent neuronal loss and cognitive impairment after permanent ischemia.

*Journal of Cerebral Blood Flow & Metabolism* (2015) **35,** 1249–1259; doi:10.1038/jcbfm.2015.55; published online 8 April 2015

**Keywords:** angiogenesis; bilateral common carotid artery occlusion; MRI cerebral blood flow; neuronal degeneration; vertebral artery

## INTRODUCTION

Bilateral common carotid artery occlusion (BCCAO) has been widely used recently as a model of vascular dementia due to chronic cerebral hypoperfusion (CCH). It has been reported that BCCAO induced loss of neurons and glial cells activation in the cortex and hippocampus, as well as learning and memory impairments in rats.[1,2] Cerebral hypoperfusion also accelerates cerebral amyloid angiopathy and promotes cortical microinfarct.[3] The damage caused by CCH not only affects cholinergic neurons, but also involves dopaminergic neurons that may contribute to the development of Parkinson's disease.[4] White-matter damage in CCH models was also reported.[5,6] Most pathologic changes were elicited when BCCAO was induced simultaneously at both common carotic arteries (CCAs). Another model was later developed in which BCCAO was induced with 1-week interval between the first and second CCA occlusions.[7] The latter allows gradual development of CCH within the brain. Although the pathologic mechanisms of these models have been widely studied, dynamic changes in cerebral blood flow (CBF) and angiogenesis are not completely understood.

Techniques for detecting CBF are primarily divided into invasive and noninvasive methodologies. The invasive techniques include autoradiographic 14C-iodoantipyrine technique[8,9] and laser-Doppler scanning.[10–13] As these techniques could damage brain tissues, clinical application is highly limited. In addition, it is difficult to determine dynamic changes in CBF and angiogenesis under CCH. To overcome limitations of invasive techniques, noninvasive techniques have been developed to measure CBF and analyze morphology of blood vessels. These techniques include computed tomography perfusion and magnetic resonance perfusion.[14] Although these techniques are widely used clinically in patients, they have been rarely employed in animal models due to difficulties in intravenous injection of contrast media in rats. In recent years, a new magnetic resonance imaging (MRI) technique, arterial spin labelling (ASL), has been introduced to assess perfusion of brain tissue without contrast media.[15] Therefore, it is now possible to measure CBF in rats using this technique.[16] In addition, magnetic resonance angiography (MRA) has been clinically used to investigate vascular structure and function, and also used in animal models of BCCAO.[6,16,17] Three-

[1]Department of Neurology, The First Affiliated Hospital, Jinan University, Guangzhou, China; [2]Department of Radiology, The First Affiliated Hospital, Jinan University, Guangzhou, China; [3]GHM Institute of CNS Regeneration (GHMICR), Jinan University, Guangzhou, China; [4]Department of Human Anatomy, Jinan University School of Medicine, Guangzhou, China and [5]Co-innovation Center of Neuroregeneration, Nantong University, Jiangsu, China. Correspondence: Dr Li'an Huang, Department of Neurology, The First Affiliated Hospital, Jinan University, Guangzhou, Guangdong 510632, China and Dr Yiwen Ruan, GHM Institute of CNS Regeneration (GHMICR), Jinan University, Guangzhou, Guangdong 510632, China.
E-mails: tlian@jnu.edu.cn and tyiwen@jnu.edu.cn
[6]These authors contributed equally to this work.
This work was supported by grants from the National Nature Science Foundation of China (Grant Nos. 81271280 and 30971530), the science and technology plan projects of Guangdong province (Grant No. 2011B05030012), National Basic Research Program 973 project (2011CB707501) and The 111 project (B14036).
Received 2 November 2014; revised 19 February 2015; accepted 10 March 2015; published online 8 April 2015

dimensional time-of-flight MR angiography (3D TOF-MRA) provides excellent spatial resolution in three directions with a better signal-to-noise ratio. It has also been recently applied to the clinic, but has hardly been utilized in animal models. Dynamic changes in vascular plasticity remain unclear.

Angiogenesis after CCH reflects a compensatory mechanism to lower CBF. Many studies have reported that BCCAO induces angiogenesis in brain.[17–19] However, dynamic changes in vascular plasticity and its mechanisms remain unknown. Therefore, the present study aimed to investigate dynamic changes in CBF and potential mechanisms underlying CCH induced by two-step BCCAO model using new MRI techniques and immunochemistry methods. We also studied neuronal degeneration and cognitive impairment induced by CCH.

## MATERIALS AND METHODS

### Animals

Adult male Wistar rats (300 to 320 g at the beginning of the study, 3.5 months) were used. All rats were housed in cages under controlled temperature (21 ± 1°C) and humidity (55 ± 10%), with a 12-hour light/12-hour dark cycle (light between 0800 and 16 00 hours). Food and water were available *ad libitum* throughout the study. All animal procedures were performed in strict accordance with the recommendations in the Guide for the Care and Use of Laboratory Animals of the National Institutes of Health. The protocol was approved by competent ethics committees at Jinan University. All efforts were made to minimize the suffering and number of animals used.

### Bilateral Common Carotid Artery Occlusion Model

Rats ($n = 40$) were anesthetized with 10% chloral hydrate (0.35 mL/100 g). A ventral right incision in the neck was performed to expose the right common carotid artery (RCCA), which was carefully separated from the adjacent vagus nerves and ligated with two 3-0 sutures. The left common carotid artery occlusion (LCCAO) was performed in the same way at 1 week after RCCA occlusion (RCCAO).

### Magnetic Resonance Imaging

Twenty rats were scanned with MRI for seven times starting at preocclusion, then at RCCAO, BCCAO, 2, 3, 4, and 6 weeks after BCCAO. The MRI experiments were conducted with a Discovery 750 3.0T scanner with an 8-channel wrist coil (GE Healthcare, Milwaukee, WI, USA). Animals were anesthetized with 10% chloral hydrate (0.3 mL/100 g) and placed in a supine position before scanning.

Imaging parameters for 3D ASL series were as follows: field of view = 120 mm × 120 mm, matrix = 512 (points) × 12 (arms), 15 slices acquired in ascending order, slice thickness = 4 mm, no gap between slices, labelling duration = 1,650 ms, postlabelling delay = 1,025 ms, repetition time = 4,132 ms, echo time = 11 ms, number of excitation = 5, bandwidth = 62.5 kHz, scan duration was 9 minutes 14 seconds.

Time-of-flight angiography with a 3D Fast SPGR was performed for quantification of vascular diameters. Scan parameters were as follows: echo time = 3.9 ms, repetition time = 20 ms, field of view = 80 mm × 60 mm, matrix = 320 × 224, number of excitation = 1, bandwidth = 31.2 kHz, and scan duration was 231 seconds.

### 3D Arterial Spin Labelling Quantification

3D ASL sequence was applied with pseudo-continuous labelling radio frequency pulse for 1.5 seconds and the postlabelling delay was 1,025 ms. An interleaved 3D stack of spiral fast spin echo sequence was used to acquire control and labelling images. For CBF quantification, a proton density weighted image was also acquired as a reference. Cerebral blood flow was calculated with the following equation:

$$CBF = \frac{\lambda\left(1-e^{\frac{-t_{sat}}{T_{1g}}}\right)}{2\alpha T_{1b}\left(1-e^{\frac{-\tau}{T_{1b}}}\right)}\ \frac{PW}{PD}e^{\frac{-PLD}{T_{1b}}}$$

In the equation, $T_{1b}$ was $T_1$ of blood (1,600 ms); $T_{1g}$, $T_1$ of gray matter (1,200 ms); $\alpha$, the labelling efficiency (0.95); $\lambda$, the cortex–blood partition coefficient (0.9); $t_{sat}$, the time of saturation performed before imaging (2,000 ms); $\tau$, the labelling duration (1,500 ms); and PLD, the postlabelling delay time.

### Image Processing

Cerebral blood flow maps were automatically calculated by commercially available scanner software (Functool 3D ASL, Software version 4.5, GE Medical Systems, Milwaukee, WI, USA). The CBF images were drawn in the parietal cortex, basal ganglion, and cerebellum of each hemisphere. The 3D-TOF angiography was postprocessed using maximum intensity projection for image processing and visualization.

### Tissue Preparation

Twenty rats were allocated into five groups (4 rats per group, $n = 4$) including sham, 2, 3, 4, and 6 weeks after BCCAO groups. After anesthetization with the same anesthetics, rats were transcardially perfused with physiologic saline followed by 4% paraformaldehyde in 0.1 mol/L phosphate-buffered saline (PBS) (pH = 7.4). Brains were removed from the skull and postfixed in the same fixative at 4°C overnight. Two transverse cuts were made parallel to the anterior and posterior lines of the hypothalamus under the inferior surface of the brain. The anterior and middle block contained the striatum and parietal cortex. Cerebellar blocks were obtained by cutting the midline of the cerebellum longitudinally. These blocks were processed for dehydration and penetration by an Automated Tissue Processor (LYNX II, Hatfield, PA, USA), and embedded with paraffin in a Thermo Scientific HistoStar (Kalamazoo, MI, USA). Sections at 10 $\mu$m thickness were cut with a paraffin microtome (Leica, RM2235, Wetzelar, Germany). Sections were mounted on slides.

### Immunofluorescent Staining and HE Staining

Sections were processed for immunofluorescence staining with CD34 antibody to label microvessels, NeuN antibody to label neurons, Iba1 and GFAP antibodies to label microglia and astrocytes. Briefly, sections were boiled to recovered antigen in 0.01 mol/L citrate buffer (pH 6.0) at 96°C to 98°C for 15 minutes. Nonspecific binding sections were blocked with 5% normal goat serum or donkey serum in PBS at room temperature for 2 hours. Sections were then incubated with CD34 antibody (from rabbit, 1 : 200, Boster, Wu Han, China) and NeuN antibody (from rabbit, 1 : 1,000, Abcam, British) separately; Iba1 antibody and GFAP antibody (from goat or from mouse, 1 : 1,000, Abcam, Cambridge, MA, USA) for double-labelling overnight at 4°C. After PBS washes, the sections were incubated with secondary antibody (Alexa Fluor 488-conjugated goat anti-rabbit IgG or donkey anti-rabbit, or donkey anti-mouse and Alexa Fluor 546-conjugated donkey anti-goat, Jackson Immunoresearch, West Grove, PA, USA) at 37°C for 2 hours. The concentration of all secondary antibodies was 1 : 1,000, then washed in PBS three times (5 minutes each) and covered with anti-quenching fluorescence mounting medium. The sections of cerebellum were performed a regular HE staining process.

### Morris Water Maze

Rats ($n = 10$ in each group) were performed a memory testing with Morris water maze. In this water navigation task, rats were first received a swimming training for 2 minutes in the first day. In the following four consecutive days, rats were performed a learning trial to escape water by finding an invisible platform under water for 1.5 cm. The swimming pool was marked with four starting positions in four quadrants equally. Each rat was randomly placed into water at one of four starting positions facing the wall of the water pool in each trial and was allowed to swim for 60 seconds. If the animal did not find the platform within 60 seconds, then the rat was gently guided to the platform and left on it for 15 seconds. Each rat was orderly performed four trials at the different four starting positions each day with an interval of 15 seconds. At the 6 days of training, rats were performed a probe trial when the platform was removed within 60 seconds separately. The escape latency to find the platform in the learning trial and the travel path in the probe trial of rats were monitored and analyzed by a video camera linked to an animal behavioral recording system (Ethovison XT, Noldus Information Technology Co., The Hague, The Netherlands).

### Quantitative Analysis

1. Cerebral blood flow. A region of interest approximate 2 $mm^2$ was selected from bilateral parietal cortex, striatum, and cerebellum. A total of 60 regions of interest from these areas in each group were analyzed.
2. Vertebral arteries (VAs). Diameters and areas of both VAs were measured at the middle of the cervical region. A total of 50 to 60 numerical values of diameters or areas in each group were analyzed.
3. CD34-positive microvessels, NeuN-postive cells, Iba1-poistive and GFAP-positive cells. A total of 40 sections contained the parietal cortex; striatum and cerebellum with a 100-$\mu$m interval between sections from each group were selected for immunofluorescent staining or for hematoxylin and eosin (HE) staining. Digital images were captured under $\times 400$ magnifications from bilateral parietal cortex, striatum, and cerebellum. There were 40 to 60 photos from each group utilized for quantitative analysis. The number of microvessels (MVN), neurons and microglia in each image was counted macroscopically. The number of astrocytes was determined by measuring the signal pixels of GFAP-positive areas with Photoshop (CS5). The area of microvessels (MVD) was defined by measuring signal pixels of CD34-positive areas using the same software. The size of each photo was approximate 0.077 $mm^2$. Measurement was performed by two individuals blinded to the samples.
4. The number of cells of the cerebellum in different groups was defined by measuring the thickness of granular layer. After HE staining, 25 to 30 cerebellar sections from each group were photographed using under $\times 400$ magnification. Approximate 50 to 60 photos from each group were analyzed. The size of each photo was approximate 0.02 $mm^2$.

### Statistical Analysis

All raw data were transferred into StatView statistical analysis software (StatView 5.0, SAS Institute, Cary, NC, USA). Statistical analysis was performed with unpaired comparisons followed by a *t*-test. A *P*-value of $< 0.05$ was considered as statistically significant. All values are presented as mean ± s.e.m.

## RESULTS

### Changes in Cerebral Blood Flow After Bilateral Common Carotid Artery Occlusion

Cerebral blood flow was measured in the cortex, striatum, and cerebellum of rats pre-occlusion, at RCCAO, BCCAO, 2, 3, 4, and 6 weeks after BCCAO using 3D ASL. Color signals of images reflect changes of CBF in these areas (Figure 1A). In pre-occlusion animals, red signal (the strongest signal) appeared in all observation areas. After RCCAO, signal in most areas turned to blue (the weakest signal) or green. Weak signal persisted until to 2 weeks after BCCAO, but red signal remained in some areas of the cerebellum immediately after BCCAO was performed. From 3 to 6 weeks after BCCAO, red signal gradually reappeared in three observation areas.

Quantitative analysis showed the same pattern as signals shown in images (Figure 1B). Immediately after RCCAO, CBF decreased to 44.3 ± 4.4% (L) and 44.6 ± 5.4% (R) in the cortex, 50.3 ± 4.9% (L) and 44.4 ± 4.8% (R) in the striatum, and 55.8 ± 6.6% (L) and 48.5 ± 6.4% (R) in the cerebellum ($P < 0.01$, compared with pre-occlusion group). Similar lower level of CBF remained till to 2 weeks after BCCAO. But it returned to 60.4 ± 5.4% in the right cortex, and 65.6 ± 4.8% in the right striatum, which was significantly higher than the left sides ($P < 0.05$ and $P < 0.01$, versus left sides) at 2 weeks although it is still lower than pre-occlusion levels ($P < 0.01$). In the cerebellum, CBF in both hemispheres returned to pre-occlusion levels immediately after BCCAO ($P > 0.05$, versus pre-occlusion). But it decreased to a lower level again at 2 weeks after BCCAO in bilateral cerebellum ($P < 0.01$, compared with pre-occlusion). Cerebral blood flow of both sides in these three areas increased to the pre-occlusion level from 3 to 6 weeks ($P > 0.05$, versus pre-occlusion) after BCCAO.

### Changes in Vertebral Artery Size After Bilateral Common Carotid Artery Occlusion

To investigate whether VAs morphologically changed after BCCAO, we used an MRA technique to measure diameters of VAs. Morphologic changes of VAs in different groups were shown in Figure 2A. Both CCAs were clearly seen in pre-occlusion group (Figure 2A-, arrows). After RCCAO, the RCCA signal disappeared (Figure 2B-, arrow head), while the LCCA was still visible (Figure 2B-, arrow). After BCCAO, both CCA signals were absent, but both VAs were still seen (Figure 2C-, arrows). From 2 to 6 weeks after BCCAO, VA diameter gradually enlarged (Figure 2D-, E- & G-, arrows).

Quantitative data of VAs were consistent with the morphologic changes (Figures 2B and 2C). The diameter of VA was 0.48 ± 0.02 mm (L), and 0.43 ± 0.02 mm (R) in the pre-occlusion group (Figure 2B). These values did not change in bilateral VAs immediately after RCCAO. However, diameter of VAs increased to 0.54 ± 0.02 mm (L) ($P < 0.01$, versus RCCAO group) and 0.64 ± 0.05 mm (R) ($P < 0.01$, versus pre-occlusion and RCCAO groups) at the time immediately after BCCAO. The left VA diameter gradually increased to 0.620 ± 0.049 mm at 2 weeks ($P < 0.01$, versus BCCAO group), 0.683 ± 0.031 mm at 3 weeks ($P < 0.01$, versus 2-week group) and 0.667 ± 0.021 mm at 4 weeks ($P < 0.01$ versus pre-occlusion group), and reached a peak value (0.867 ± 0.047 mm, $P < 0.01$ versus 3- and 4-week groups) at 6 weeks after BCCAO. The right VA diameter increased to 0.51 ± 0.01 mm at the time immediately after BCCAO ($P < 0.01$ versus the pre-occlusion and RCCAO groups), 0.640 ± 0.060 mm at 2 weeks ($P < 0.01$ versus BCCAO groups), 0.683 ± 0.031 mm at 3 weeks, and 0.683 ± 0.017 mm at 4 weeks, and reached a peak value (0.883 ± 0.069 mm, $P < 0.01$ versus 3- and 4-week groups) at 6 weeks after BCCAO.

The pattern of change in VA area was similar to that in VA diameter (Figure 2C). The area of pre-occlusion group was 0.227 ± 0.009 $mm^2$ (L), 0.200 ± 0.007 $mm^2$ (R). It did not change when RCCAO was induced. But it significantly increased to 0.315 ± 0.021 $mm^2$ (L) and 0.261 ± 0.01 $mm^2$ (R) when BCCAO was performed, ($P < 0.01$ versus the pre-occlusion and RCCAO groups). Then, the size of VAs gradually increased at 3 and 4 weeks, and reached a peak value (0.621 ± 0.058 $mm^2$ (L) and 0.642 ± 0.092 $mm^2$ (R) ($P < 0.01$ versus 3-week group) at 6 weeks after BCCAO).

### Changes in Number and Area of Microvessels After Bilateral Common Carotid Artery Occlusion

To investigate whether angiogenesis may be activated after BCCAO, we used CD34 (an endothelial cell marker) immunofluorescence to detect changes in microvessels in the parietal cortex, striatum, and cerebellum (Figure 3A, arrows).

Quantitative analysis in these three areas was consistent with the results shown in Figure 3A. In the parietal cortex (Figure 3B), the MVN in the left side (LMVN) reduced to 37.3 ± 3.8% at 2 weeks, 25.7 ± 2.2% at 3 weeks, and 44.8 ± 4.8% at 4 weeks after BCCAO (all $P < 0.01$ versus sham). However, it returned to the sham level (89.2 ± 6.0%, $P > 0.05$) at 6 weeks after BCCAO. To understand changes in microvessel areas, we used pixel signal to measure positive staining areas. The changing pattern of microvessel pixel signal in the left side (LMVD) paralleled to the LMVN. After BCCAO, LMVN reduced to 48.7 ± 6.1% at 2 weeks, 45.8 ± 7.0% at 3 weeks, and 56.6 ± 6.0% at 4 weeks after BCCAO (all $P < 0.01$ versus sham). However, the numbers returned to the sham level (127.5 ± 10.1%, $P > 0.05$) at 6 weeks after BCCAO. The MVN in the right side (RMVN) and the MVD in the right side (RMVD) in the right parietal cortex underwent the resembled changes. It reduced to 63.8 ± 5.2% at 2 weeks, 44.9 ± 5.1% at 3 weeks and 65.4 ± 6.0% at 4 weeks after BCCAO (all $P < 0.01$ versus sham), then increased to 1.4-fold sham level (142.2 ± 5.2%, $P < 0.01$ versus sham). The RMVD reduced to 43.42 ± 5.6% at 2 weeks, 28.9 ± 4.5% at 3 weeks,

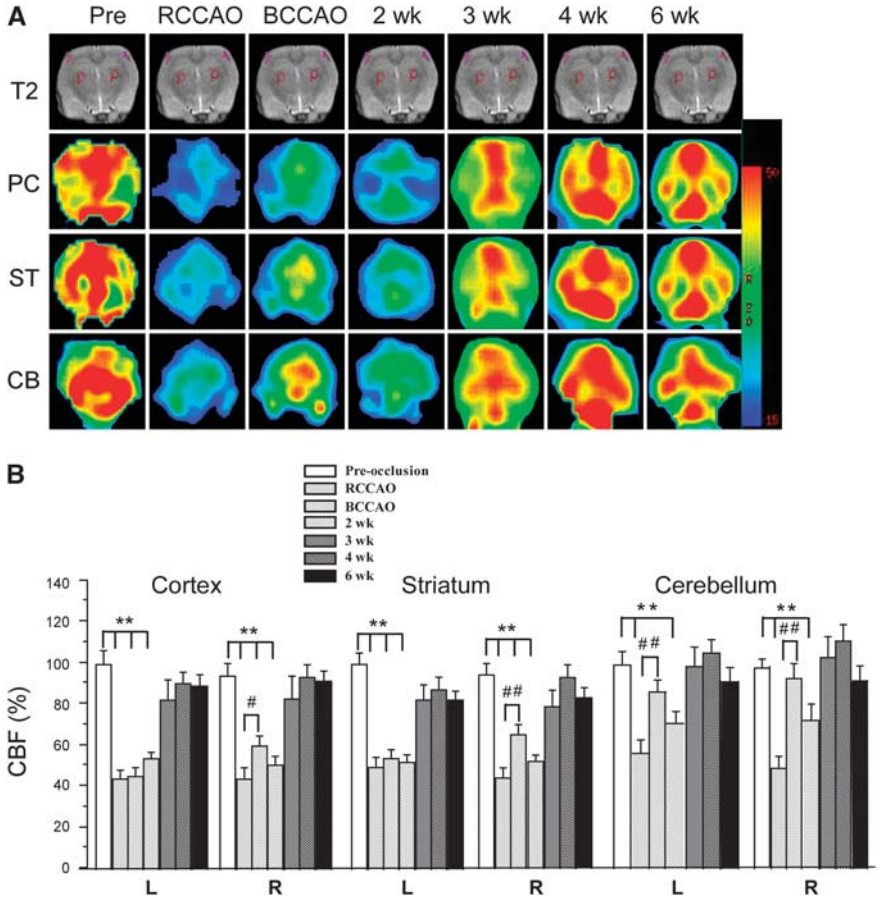


**Figure 1.** Magnetic resonance imaging (MRI) images showing changes in cerebral blood flow (CBF) of the parietal cortex (PC), striatum (ST), and cerebellum (CB). Color images are from 3D arterial spin labelling (ASL) and gray images from T2 MRI (**A**). Areas in red in ASL images represent the strongest signal of CBF; and areas in blue or green reflect the weakest signal of CBF; and the yellow color is intermediate signal between them. Pink or red circles indicate detected areas of CBF in the parietal cortex and striatum. Histogram showing quantitative results of CBF at different time points after bilateral common carotid artery occlusion (BCCAO) (**B**). CBF of bilateral parietal cortex, striatum, and cerebellum decreased at right common carotid artery occlusion (RCCAO), BCCAO, and 2 weeks after BCCAO, compared with pre-occlusion ($P < 0.01$). But it increased in the right parietal cortex ($P < 0.05$), right striatum ($P < 0.01$) and both cerebellar hemispheres ($P < 0.01$) compared with RCCAO group when BCCAO was induced. CBF of these three areas returned to the pre-occlusion level from 3 to 6 weeks after BCCAO. $^{**}P < 0.01$; $^{\#}P < 0.05$; $^{\#\#}P < 0.01$.

and 65.2 ± 6.5% at 4 weeks after BCCAO (all $P < 0.01$ versus sham), and increased to 137.9 ± 11.2% ($P < 0.05$ versus sham) at 6 weeks after BCCAO.

In the striatum (Figure 3C), the percentage of LMVN and LMVD decreased to 65.2 ± 3.5% and 56.7 ± 8.2% at 2 weeks, 64.8 ± 7.2% and 41.2 ± 10.2% at 3 weeks, and 54.8 ± 6.1% and 30.5 ± 6.1% at 4 weeks after BCCAO (all $P < 0.01$ versus sham), then it returned to the sham level (87.6 ± 8.8% of LMVN, 107.2 ± 20.2% of LMVD, $P > 0.05$ versus sham) at 6 weeks after BCCAO. In the right striatum, RMVN and RMVD decreased to 68.7 ± 3.2% and 65.7 ± 9.2% ($P < 0.01$) at 2 weeks, 70.0 ± 4.2% and 57.7 ± 11.23% ($P < 0.01$) at 3 weeks, 51.7 ± 5.2% ($P < 0.01$), and 62.7 ± 8.9% ($P < 0.05$) at 4 weeks after BCCAO compared with sham group. Values returned to sham level (91.2 ± 6.9% and 122.3 ± 28.8%, $P > 0.05$) at 6 weeks after BCCAO.

For the cerebellum (Figure 3D), LMVN, LMVD, RMVN, and RMVD reduced to 78.1 ± 3.9%, 32.3 ± 3.4%, 63.4 ± 2.9%, and 51.7 ± 6.5% at 2 weeks, and remained at a lower level (65.9 ± 3.4%, 26.7 ± 2.9%, 48.2 ± 5.6%, and 47.2 ± 10.5%) at 3 weeks (all $P < 0.01$ compared with sham). However, the value increased to the control level at 4 weeks after BCCAO (all $P > 0.05$ versus sham). The MVN and the MVD maintained at sham levels except for elevated RMVN (110.2 ± 4.2%, $P < 0.05$ versus sham) at 6 weeks after BCCAO.

### Changes in Numbers of Neurons and Glial Cells After Bilateral Common Carotid Artery Occlusion

To reveal whether the compensation in CBF and blood vessels would affect the recovery of neuronal morphology after BCCAO, we investigated numbers of neurons and glial cells before and after ischemia by immunofluorescent staining. The morphologic changes of neurons (NeuN-postive cells), microglial cells (Iba1-positive cells), and astrocytes (GFAP-positive cells) in the parietal cortex were shown in Figure 4A (arrows and arrowhead).

Quantitative analysis revealed that the number of NeuN-positive cells dramatically decreased to 55.8 ± 2.3%, 57.0 ± 2.7%, 51.28 ± 2.4%, and 48.15 ± 1.5% in the left parietal cortex (all $P < 0.01$ versus sham), 57.24 ± 2.3%, 56.49 ± 2.7%, 49.44 ± 2.1%, and 49.33 ± 1.7% in right parietal cortex (all $P < 0.01$ versus sham) from 2 weeks to 6 weeks after BCCAO (Figure 4B). However, the numbers of Iba1-positive cells did not significantly change at 2 and 3 weeks, but dramatically increased to 287.90 ± 51.7% (L), 200.37 ± 31.2% (R) ($P < 0.01$ and $P < 0.05$ versus sham) at 4 weeks, and then returned to the sham level at 6 weeks ($P > 0.05$ versus sham) after BCCAO (Figure 4C). The number of GFAP-positive cells did not show a significant decrease at 2 and 3 weeks, but significantly increased to 292.47 ± 37.9% (L), 265.76 ± 51.7% (R) at

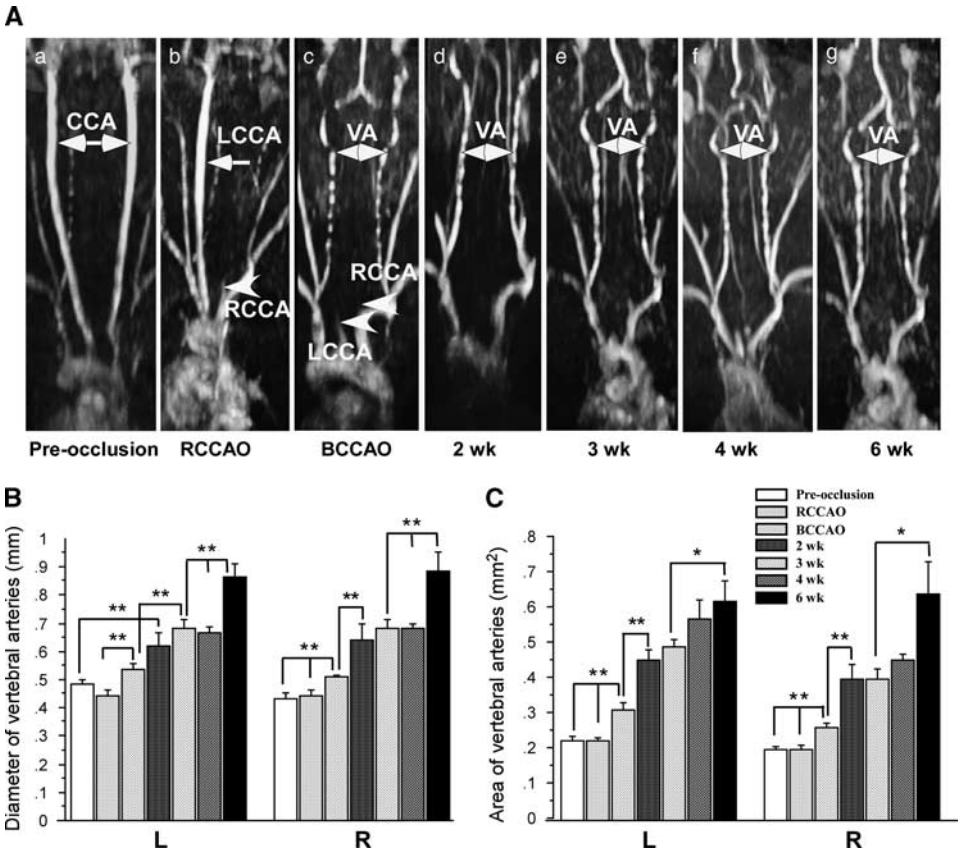


**Figure 2.** Changes in bilateral common carotid arteries (CCAs) and vertebral arteries (VAs) before and after bilateral common carotid artery occlusion (BCCAO). Three-dimensional time-of-flight MR angiography (3D TOF-MRA) images showing morphologic changes of CCAs and VAs (**A**). In pre-occlusion rats, bilateral CCAs were clearly seen (A-, arrows). After RCCA was occluded, its signal disappeared from the image (B-, arrow head), but LCCA was still visible (B-, arrow). After BCCAO, both CCA signals were absent from the image (C-, arrow head). At the same time, bead-like VAs were seen (C-, arrows). Gradual enlargement of VAs was observed from 2 to 6 weeks after BCCAO (D-, E-, and F-, arrows). Histogram showing changes in diameter and area of bilateral VAs (**B**, **C**). There was no difference in diameter and area of VAs between pre-occlusion group and right common carotid artery occlusion (RCCAO) group. The diameter of both VAs increased at 1 week after RCCAO when BCCAO was induced ($P < 0.01$ versus RCCAO group in the left VA, $P < 0.01$ versus the pre-occlusion and RCCAO groups in the right VA). VAs gradually became larger from 2, 3, and 4 weeks, and peaked at 6 weeks after BCCAO. Changes in VA area also underwent a similar pattern as that for VA diameter after BCCAO. $^{**}P < 0.01$; $^{*}P < 0.05$ compared with sham.

4 weeks, and 260.76 ± 52.7% (L), 218.50 ± 31.7% (R) at 6 weeks after BCCAO, all $P < 0.01$ versus sham (Figure 4D).

The morphologic changes of neurons and glial cells in the striatum before and after BCCAO were shown in Figure 5A. Quantitative analysis showed that changes in the number of neurons in the striatum resembled that in the parietal cortex. The number of NeuN-postive cells dramatically decreased to approximate 50% from 2 to 6 weeks after BCCAO, all $P < 0.01$ compared with sham (Figure 5B). The numbers of Iba1-positive cells was first dramatically declined to 10.0 ± 5.6% (L), 11.1 ± 6.1% (R) both $P < 0.01$ versus sham at 2 weeks after BCCAO. It then gradually increased and reached to 170.47 ± 30.3% (L), 171.15 ± 38.27% (R) at 4 weeks, 194.76 ± 59.1% (L) 197.72 ± 45.97% (R) at 6 weeks after BCCAO, all $P < 0.01$ versus sham (Figure 5C). The number of GFAP-positive cells first decreased to 34.8 ± 12.7% (L), 39.7 ± 8.2% (R), both $P < 0.01$ versus sham at 2 weeks (Figure 5D). Then it gradually increased and reached a peak value to 160.3 ± 112.0% (L) and 160.2 ± 116.7% (R), both, $P < 0.01$ versus sham at 4 weeks and then declined to the sham level in both sides at 6 weeks.

For cerebellum, we first measured the thickness of granular layer to evaluate the number of cells by HE staining (Figure 6A). It turned out that there was no difference between sham and other ischemic groups (Figure 6B). Therefore, we did not further investigate changes in different cell types.

## Changes in Learning and Memory After Bilateral Common Carotid Artery Occlusion

After we found that CCH induced neuronal degeneration, we further investigated whether two-step BCCAO model in our study would induce cognitive impairment. Rats were trained to perform Morris water maze. In the first learning trial (Figure 7A), the escape latency in the sham group was 36.2 ± 2.5 seconds in day 1. After surgery, it significantly prolonged to 48.3 ± 2.7 seconds , 53.0 ± 1.9 seconds, and 54.7 ± 2.2 seconds at 2, 4, and 6 weeks after BCCAO, all $P < 0.01$ compared with sham. In day 2, although there was no difference between the sham, postischemic 2- and 4-week groups, the escape latency was prolong in ischemic 6-week group, $P < 0.01$ versus sham. In day 3, the escape latency was 32.5 ± 2.9 seconds at ischemic 2-week group ($P < 0.05$), 33.1 ± 1 seconds ($P < 0.05$) at ischemic 4-week group and 42.3 ± 2.4 seconds ($P < 0.01$) at ischemic 6-week group, compared with sham (24.3 ± 4.6 seconds ). The record of escape latency in day 4 was similar to day 3.

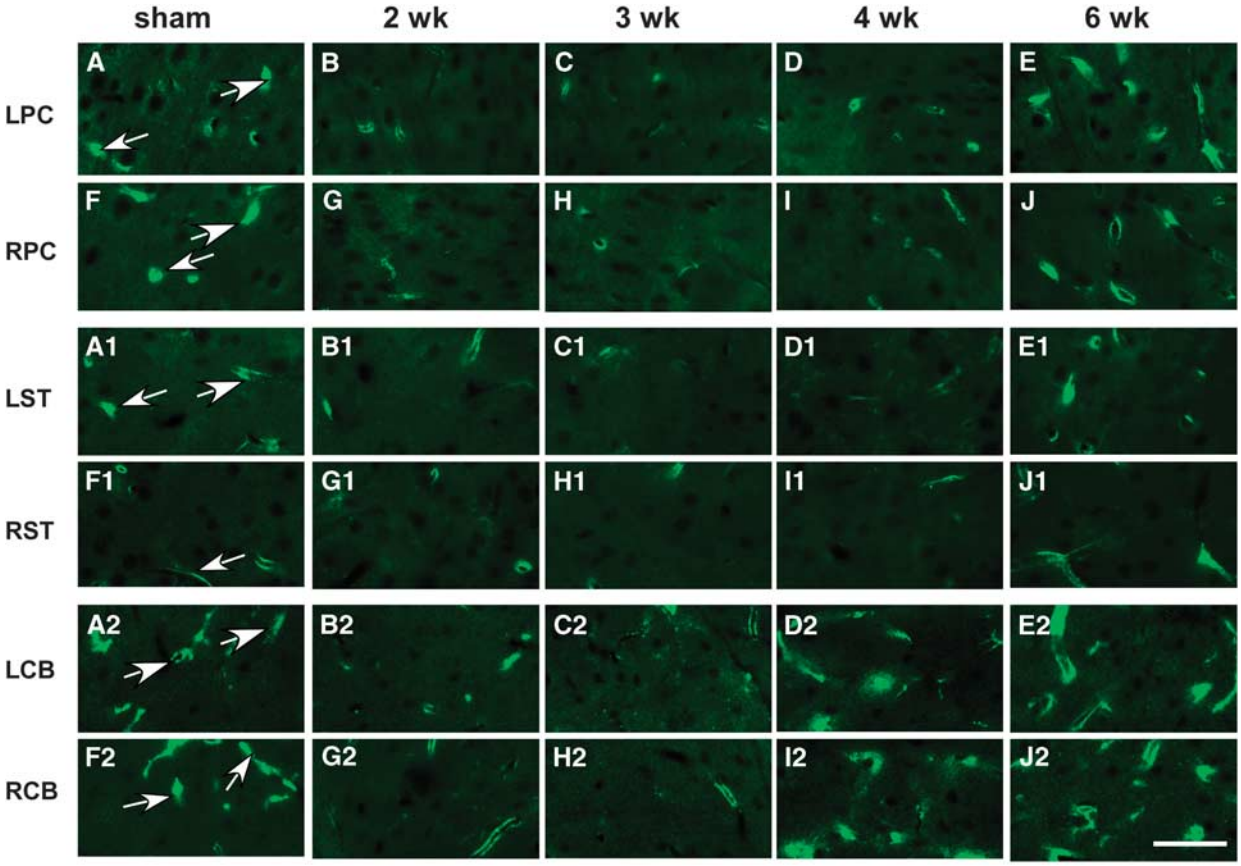


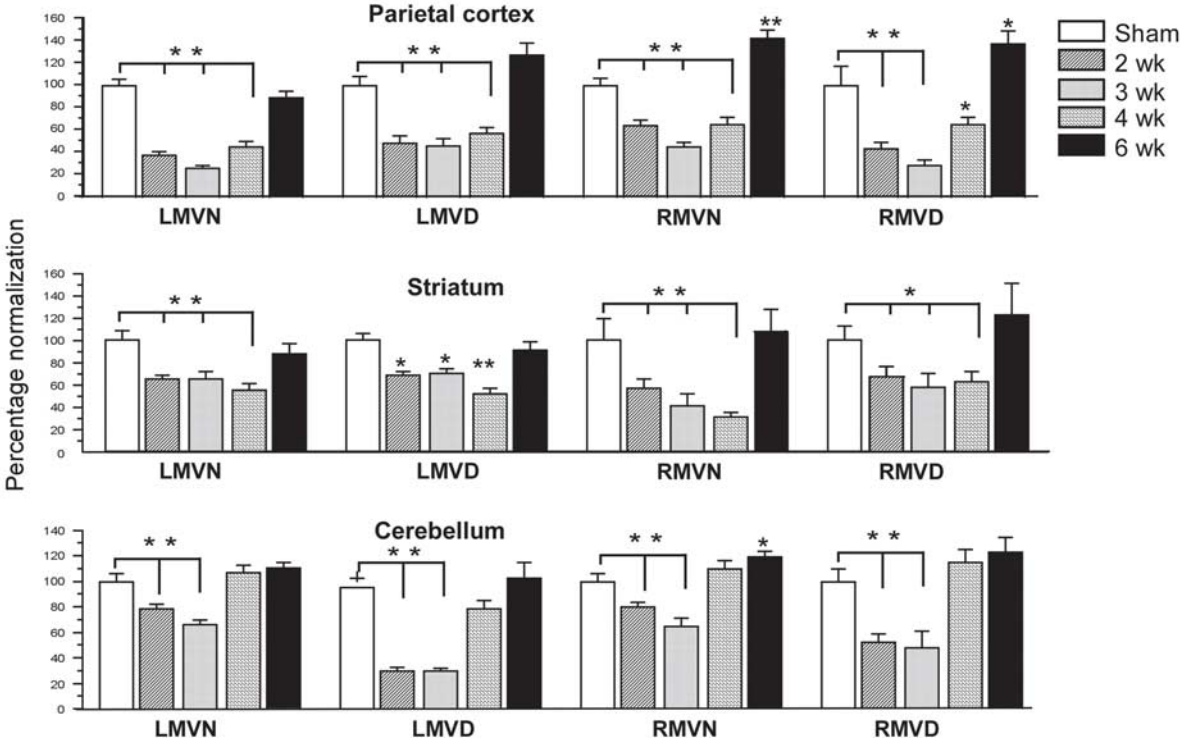


In the probe trial, the platform was removed. Rats were allowed to navigate in water for 60 seconds. The travel path crossing the original platform was recorded (Figure 7B, the circle represented the platform). Quantitative data showed that the frequency crossing the original platform was $2.4 \pm 0.3$ in the sham group, $2.1 \pm 0.2$ at 2-week, $1.3 \pm 0.3$ at 4-week, and $0.8 \pm 0.2$ at 6-week groups after BCCAO ($P < 0.01$ compared with the sham and 2-week groups, Figure 7C). The duration spent in the platform

**Figure 3.** Morphologic changes in microvessels. Micrograph showing CD34 immunofluorescence staining of microvessels in the parietal cortex, striatum, and cerebellum at different points after bilateral common carotid artery occlusion (BCCAO) (**A**). In the sham group, stronger staining of CD34-positive microvessels was seen in the parietal cortex (A- and F, arrows), striatum (A1 and F1, arrows) and cerebellum (A2 and F2, arrows). However, the staining signal reduced at 2 weeks (B-, G, B1, G1, B2, G2) and 3 weeks (C-, H, C1, H1, C2, H2) in these three areas, and 4 weeks (D-, I, D1, I1) after BCCAO in the parietal cortex and the striatum. Stronger labelled CD34-positive microvessels reappeared earlier in the cerebellum at 4 weeks (D2, I2) and later at 6 weeks (E-, J, E1, J1, E2, J2) in the parietal cortex and the striatum after BCCAO. LPC, left parietal cortex; RPC, right parietal cortex; LST, left striatum; RST, right striatum; LCB, left cerebellum; RCB, right cerebellum. Histogram showing quantitative data (**B**–**D**): In the left parietal cortex, the percentage of the number and areas of microvessels decreased at 2, 3, and 4 weeks ($P < 0.01$) and returned to the sham level at 6 wk ($P > 0.05$). (**B**) In the right parietal cortex, the percentage of the number and areas of microvessels also decreased at 2, 3, and 4 weeks ($P < 0.01$ and $P < 0.05$) but increased at 6 weeks after BCCAO (RMVN, $P < 0.01$ and RMVD, $P < 0.05$) compared with the sham group. The percentage of the number and areas of microvessels in the striatum underwent a similar changing pattern (**C**). In the cerebellum, however, the percentage of the number and areas of microvessels decreased at 2 and 3 weeks but returned to the sham level from 4 weeks after BCCAO (**D**). LMVN, the number of microvessels in the left side; LMVD, the area of microvessels in the left side. RMVN, the number of microvessels in the right side; RMVD, the area of microvessels in the right side. $^{**}P < 0.01$; $^{*}P < 0.05$ compared with sham. Scale bar, 20 $\mu$m.

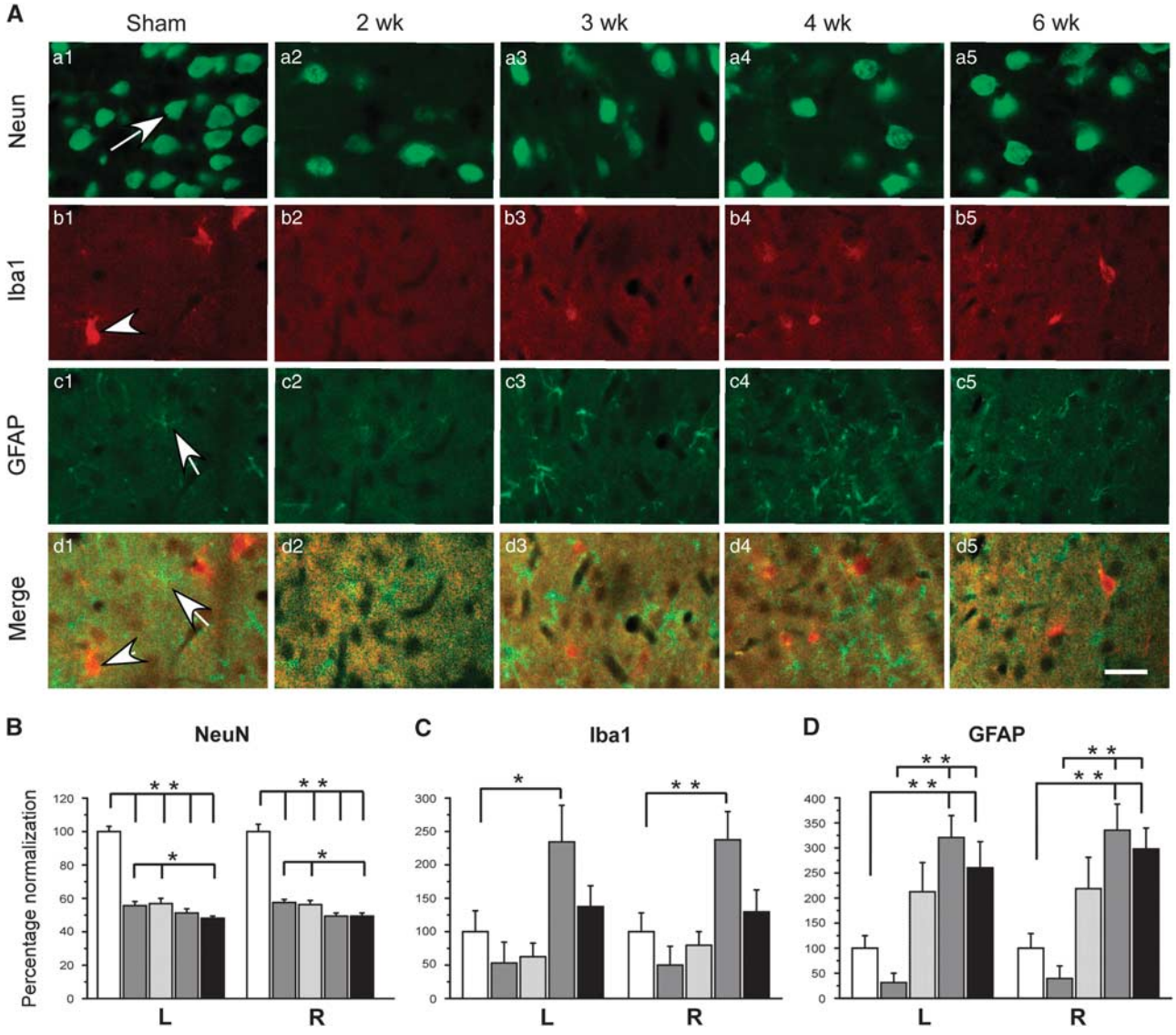


**Figure 4.** Changes in different types of cells in the parietal cortex. Micrograph showing changes of different types of cells in the parietal cortex at different points after bilateral common carotid artery occlusion (BCCAO) by immunofluorescent staining (**A**). NeuN-positive cells (neurons) were found in A1 to A5 (arrow), Iba1-positive cells (microglial cells) in B1 to B5 (arrowhead), and GFAP-positive cells (astrocytes) in C1 to C5 (arrow). The later two types cells were also seen in merge pictures of Iba1 and GFAP double immunostaining (D1 to D5). Histogram showing the results of quantitative analysis (**B**–**D**). The number of NeuN+ cells dramatically decreased to a half of sham level in bilateral parietal cortex ($P < 0.01$) from 2 to 6 weeks after BCCAO (**B**). However, the numbers of Iba1+ cells did not significantly change at 2 and 3 weeks but significantly increased at 4 weeks, $P < 0.05$ (L), $P < 0.01$ (R), then returned to the normal level at 6 weeks after BCCAO (**C**). The number of GFAP + cells decreased first at 2 weeks, then gradually increased from 3 weeks and reached peak values at 4 weeks ($P < 0.01$) and 6 weeks ($P < 0.01$) after BCCAO compared with sham (**D**). $^{**}P < 0.01$; $^{*}P < 0.05$; scale bar, 20 $\mu$m.

quadrant was 20.0 ± 4.2 seconds at the sham group, 16.4 ± 6.4 seconds at 2-week, 16.4 ± 6.4 seconds at 4-weeks and 13.7 ± 5.4 seconds at 6-week groups after BCCAO (Figure 7D), which was significantly declined at all ischemic groups, $P < 0.01$ between the sham and 4- or 6-week groups, $P < 0.05$ between the sham and ischemic 2-week group.

## DISCUSSION

In the present study, we used MRI techniques to detect dynamic changes of CBF in the cortex, striatum, and cerebellum of rats at different time points after BCCAO. We also employed immunofluorescence staining to observe changes in angiogenesis and cell numbers in these three areas. Our findings revealed there was a parallel relationship between alteration of CBF and angiogenesis or size of VAs, which suggests that CCH activates a compensatory vascular mechanism attempting to maintain an optimal CBF in the brain. However, this compensation could not prevent neuronal death and cognitive impairment induced by CCH.

### Bilateral Common Carotid Artery Occlusion Models and Cerebral Blood Flow

The compensation of CBF is highly relative to the formation of collateral circulation. Clinically, a larger infarction area occurred in patients with poor collateral circulation after stroke, while light damage developed in patients with good collateral circulation.[21] Cerebral blood flow in ischemic model induced by occlusion of both left and right CCAs (one step) simultaneously was lower than that induced by occlusion of both CCAs with 1-week interval (two steps).[7,22,23] Although CBF in some areas of the brain was recovered by 4 weeks after BCCAO in one-step model, CBF in occipital cortex and globus pallidus was still lower than control levels at the stage.[23] However, in two-step BCCAO model of our

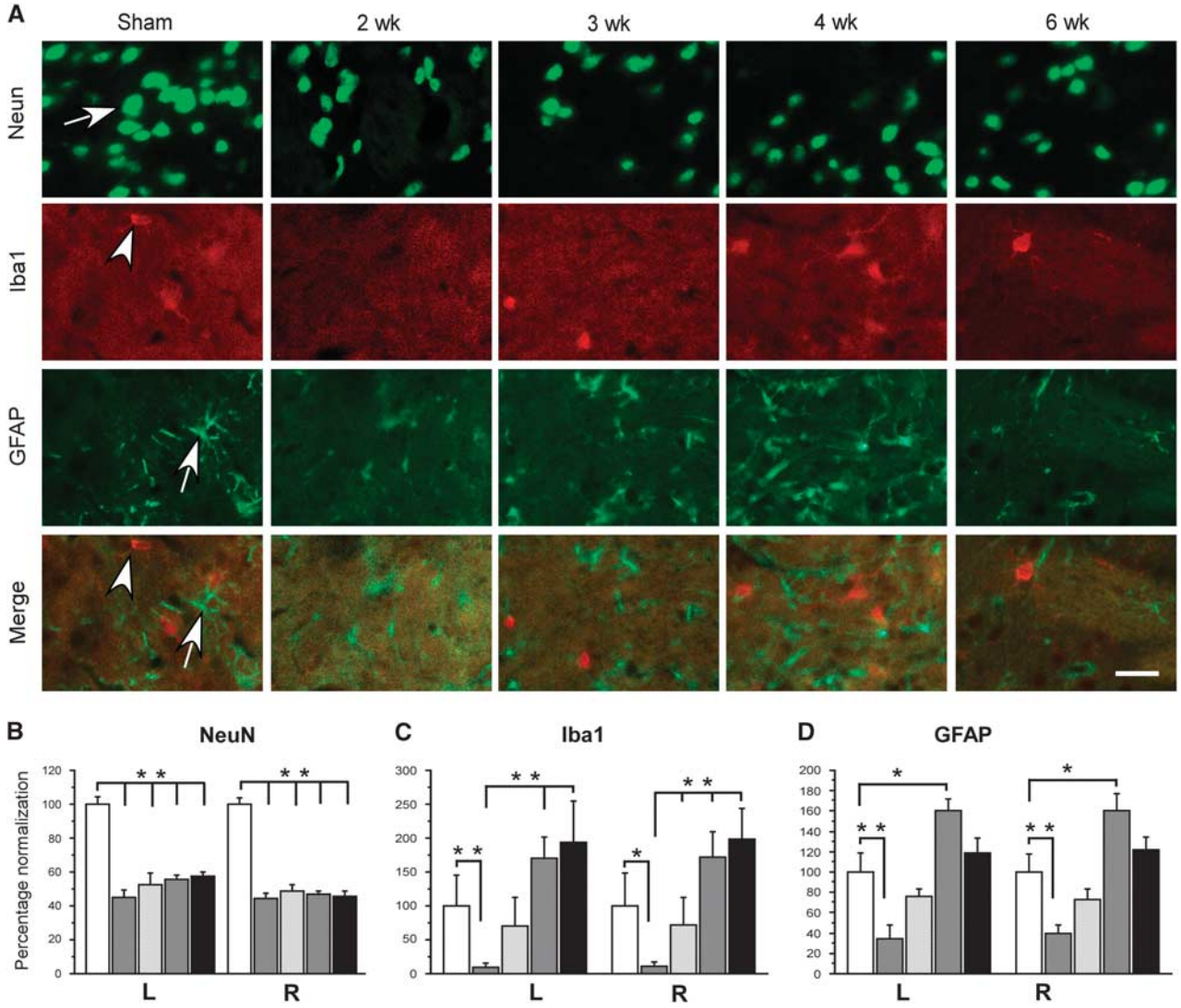


**Figure 5.** Changes in different types of cells in the striatum. Micrograph showing changes of different types of cells in the striatum at different points after bilateral common carotid artery occlusion (BCCAO) by immunofluorescent staining (**A**). NeuN-positive cells were found in A1 to A5 (arrow), Iba1-positive cells in B1 to B5 (arrow head), and GFAP-positive cells (astrocytes) in C1 to C5 (arrow). The later two types cells were also seen in merge pictures of Iba1 and GFAP double immunostaining (D1 to D5). Histogram showing the results of quantitative analysis (**B**–**D**). The number of NeuN-postive cells dramatically decreased to approximate 50% in bilateral striatum ($P < 0.01$) from 2 to 6 weeks after BCCAO (**B**). The numbers of Iba1-positive cells in both striatum also dramatically declined at 2 weeks ($P < 0.01$ at left and $P < 0.05$ at right), then gradually increased and reached peak values at 4 and 6 weeks after BCCAO compared with sham (**C**). The number of GFAP-positive cells underwent a similar changing pattern. It first decreased at 2 weeks ($P < 0.01$, **D**), then gradually increased and reached a peak value at 4 weeks ($P < 0.05$) and then returned to the sham level at 6 weeks after BCCAO ($P > 0.05$). $^{**}P < 0.01$; $^{*}P < 0.05$; scale bar, 20 $\mu$m.

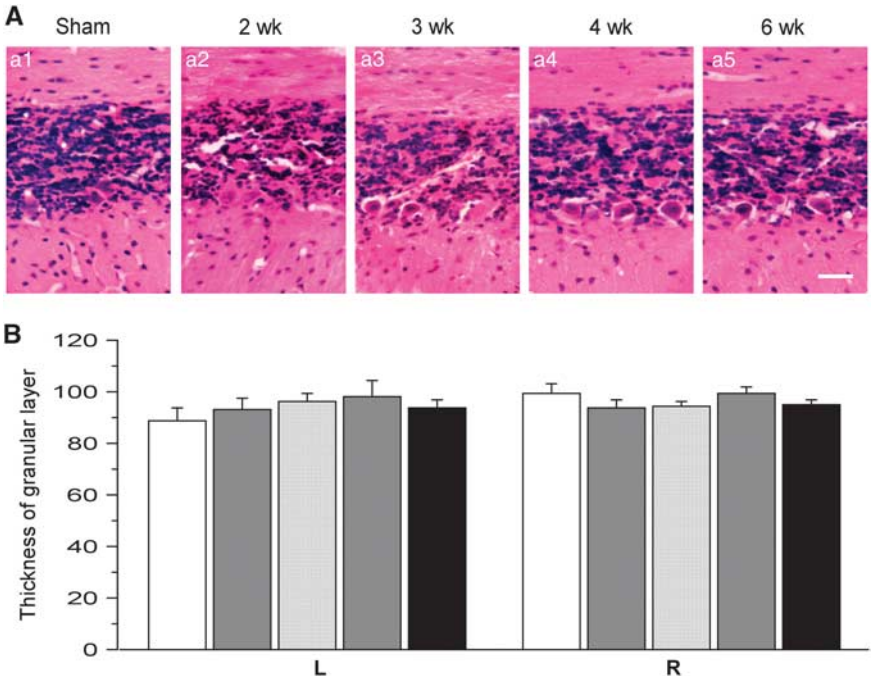


**Figure 6.** Changes in thickness of granular layer of the cerebellum. (**A**) Micrograph showed the morphologic changes of granular layer of the cerebellum by HE staining (A1 to A5). Quantitative analysis showed that there was no difference in the thickness of granular layer in the cerebellum at different points after bilateral common carotid artery occlusion (BCCAO) ($P > 0.05$, **B**), Scale bar, 20 $\mu$m.

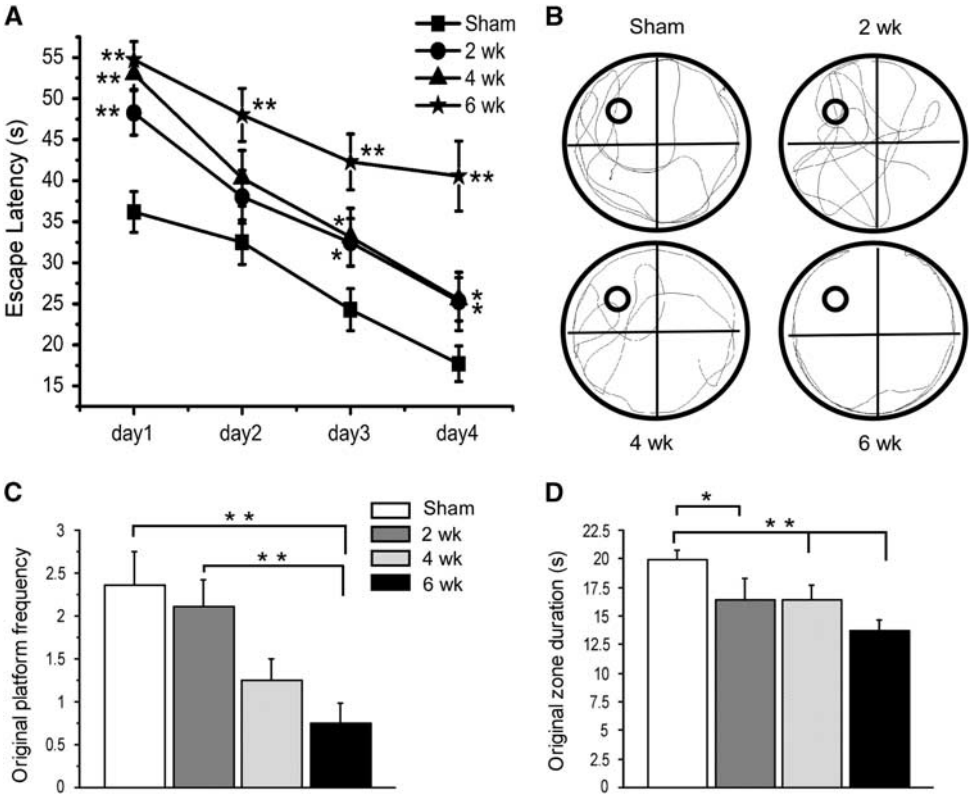


**Figure 7.** Changes in memory behavior detection. Plot graph showing changes in escape latencies in all experimental groups (**A**). In day 1, the escape latency was significantly longer in all ischemic groups ($P < 0.01$) compared with sham group. In day 2, longer escape latency was found at ischemic 6-week group ($P < 0.01$). In day 3 and day 4, the escape latency was significantly prolonged at 2- and 4-week groups ($P < 0.05$), and 6-week group ($P < 0.01$) after bilateral common carotid artery occlusion (BCCAO). The travel path of rats crossing the platform (circle) or platform quadrant was shown in (**B**). Quantitative data showed that the frequency crossing the original platform was decreased in all ischemic groups (**C**). And the duration travelling in the original platform quadrant was also declined in ischemic groups ($P < 0.05$ at 2 weeks, $P < 0.01$ at 4 and 6 weeks after BCCAO) (**D**). $^{**}P < 0.01$; $^{*}P < 0.05$, compared with sham.

study, CBF only decreased to around 50% of pre-occlusion level in the cortex, the striatum, and the cerebellum immediately after RCCAO. Although CBF in the left cortex and striatum was still reduced at the time when BCCAO was performed, the CBF of the right cortex and right striatum had returned to 60% to 65% of pre-occlusion level. Therefore, reduction of CBF in two-step BCCAO model is lesser than that in one-step BCCAO model. The time of complete CBF recovery in two-step model of our study was also earlier than that observed in one-step BCCAO model. The CBF in the three areas almost approached normal levels by 3 weeks in our study, while it took 4 weeks for a complete CBF recovery in one-step BCCAO model.[18,24–26] Clinically, artery occlusion in most of ischemic stroke patients occurs slowly. It was not often the case that bilateral common carotid arteries were suddenly occluded in stroke patients. Therefore, the pathologic mechanism of two-step BCCAO model is more close to that of ischemic stroke patients in clinical.

In addition, the CBF value in the cortex, striatum, and cerebellum maintained a similar level immediately after RCCAO, which may reflect an early compensation mechanism involving rapid redistribution of CBF to these observation areas through collateral circulation of the circle of Willis. Nonetheless, CBF compensation is insufficient at early stages after CCA occlusion because CBF in these areas was still lower than the sham at 2 weeks after BCCAO. To preserve cortical blood flow, blood in the cerebellum will flow into the cortex through the circle of Willis, which will therefore cause a lower perfusion in the cerebellum CBF at the same time. Compared with the cortex and striatum, CBF recovery in the cerebellum occurred earlier than in the cortex and striatum after BCCAO. This phenomenon may be related to reperfusion of CBF to the cerebellum directed by dilated VAs during this period.

### Possible Mechanisms Underlying Compensation of Cerebral Blood Flow

Compensation mechanisms for recovering CBF in CCH brains may be involved in biomedical regulation of CBF, recruitment of nonperfused capillaries, angiogenesis, and dilation of VAs.[17] In the present study, we observed that BCCAO activated two compensation mechanisms: dilation of VAs and angiogenesis. Our results showed that dilation of VAs first occurred 1 week after RCCAO. The diameter of both VAs gradually increased to 6 weeks after BCCAO. It has been reported that VAs, basilar artery, proximal segments of the posterior cerebral arteries, and posterior communicating artery gradually enlarge starting 4 days to 6 months after one-step BCCAO model.[18,24–26] Dilation of VAs in these studies occurred earlier than in two-step BCCAO model of our study. Therefore, changes in VAs and other compensatory arteries are determined by blood flow level: the greater the CBF decrease, the more alteration in blood vessels that takes place.

Another compensatory mechanism observed in our study is angiogenesis.[17] Angiogenesis was observed at the border of the infarction 48 to 72 hours after permanent middle cerebral artery occlusion.[27] In the two-step model, capillary densities in both frontal and parietal cortices increased to approximately 1.3-fold of the control level at 28 days after surgery, and similar results were observed in CCH mice.[28] Here, CCH induced a decrease in the microvascular number and areas within the parietal cortex, striatum, and cerebellum at 2 and 3 weeks after BCCAO. The complete recovery of microvascular number and area appeared early in the cerebellum at 4 weeks and then in the parietal cortex and striatum at 6 weeks after BCCAO. The greatest increase in microvascular density was seen in the right parietal cortex and reached approximately 1.4-fold of the control level at 6 weeks after BCCAO. Based on our results shown here, CBF recovered to the pre-occlusion level at 3 weeks after BCCAO, while delayed angiogenesis took place from 4 to 6 weeks. This suggests that compensation for CBF occurred in the early stage (2 to 3 weeks after BCCAO) was achieved primarily through VA dilation, while angiogenesis paralleled recovery of blood flow in the later stage (from 4 to 6 weeks) after BCCAO. The mechanism of dilation of VAs after BCCAO may be involved smooth muscle hyperplasia, a reduction of collagen I/III, and a decrease in myogenic tone.[16,23]

### Roles of Magnetic Resonance Imaging Techniques in Measurement of Cerebral Blood Flow and Arteries

Several MRI methods have been widely applied to clinically measure CBF in stroke patients. The most commonly used methods can be generally divided into two broad techniques:[29] ASL and dynamic-susceptibility contrast MRI.[30] The former uses magnetic labelled blood as an endogenous contrast (completely noninvasive) and the latter relies on the intravenous injection of a paramagnetic contrast agent. These techniques have been used to measure CBF in one-step BCCAO model.[6,16,31] And a good correlation in measured values of CBF between 3D ASL and dynamic-susceptibility contrast MRI techniques has previously been shown.[31,32] However, the dynamic change in CBF induced by CCH remained unclear in their studies. In recent years, new MRI techniques have been gradually developed, including continuous arterial spin labelling perfusion MRI, spiral readout (3D pASL), and 3D fast spin echo with spiral readout. These MRI techniques can enhance the signal-to-noise ratio, slice coverage, reduces motion artifacts and distortion in regions of high magnetic susceptibility.[33–36] Still, fast spin echo has not yet been applied in laboratory experiments. On the basis of the literature and our data, we determined that the 3D ASL technique had high accuracy and was more suitable for experimental animal studies.

The MRA technique has also been exclusively used in patients to image blood vessels[16,20,37] as well as in animal studies.[26] In the present study, we also obtained quality images of vasculature and measured the diameter and area of VAs using a clinical 3.0T MR scanner. Therefore, the MRA technique is a useful tool for demonstration and measurement of blood vessels in both human and animal applications.

### CCH Induces Neuronal Degeneration and Cognitive Impairment

Our results have shown that CCH induces a compensatory mechanism of CBF and blood vessels in the cortex, striatum, and cerebellum. However, this compensation could not prevent neuronal death in the cortex and striatum and cognitive impairment. Many studies have shown degeneration of different types of cells occurred in the chronic brain hypoperfusion.[1,2,4,5] Our results further supported their findings because the number of neurons in both cortex and striatum dramatically decreased from 2 to 6 weeks after BCCAO, which indicates neurons in these two areas are vulnerable to CCH. However, granular neurons in the cerebellum are resistant to CCH because the thickness of granular layer of the cerebellum did not change under CCH. The reaction of glial cells response to CCH is different in the cortex and the striatum. In the cortex, two types of glial cells were coactivated at 4 weeks after BCCAO because the number of these two types dramatically increased at this stage. Astrocytes were the main source for the accumulation of glial cells at 6 weeks after BCCAO due to the number of GFAP-positive cells was still larger, while the number of microglial cells returned to the sham level at this time. It has been reported that one-step BCCAO model induced activation of astrocytes in the cortex at 1 weeks after ischemia.[24] However, activation of astrocytes in the cortex in our study mainly occurred at 4 weeks after ischemia, which suggests that two-step BCCAO model may cause delayed activation of astrocytes in the brain.

In the striatum, the number of both microglial cell and astrocytes underwent a parallel process. It decreased first at 2 weeks, then gradually increased from 3 weeks, and reached a

peak value at 4 weeks following BCCAO. The most activated stage of glial cells is still at 4 weeks after BCCAO. But activation of microglial cells in the striatum will be longer than in the cortex because the number of microglial cells was till larger at 6 weeks after BCCAO, while the number of GFAP has returned to the sham level at this time.

Consistent with the degeneration of neurons, CCH also induced cognitive impairment in two-step BCCAO model in this study, which further confirmed the fact that CCH induces learning and memory damage from other studies.

## DISCLOSURE/CONFLICT OF INTEREST

The authors declare no conflict of interest.

## ACKNOWLEDGMENTS

The authors thank Zhenyu Zhou and Zhongping Zhang from GE Healthcare MRRC China for his support and assistance in MRI techniques, Tingting Li and Ling Zeng from GHMICR of Jinan University for the help in data analysis. We thank Clarity Manuscript Consultants LLC for assistance in editing the manuscript.

## REFERENCES

1 Xi Y, Wang M, Zhang W, Bai M, Du Y, Zhang Z *et al.* Neuronal damage, central cholinergic dysfunction and oxidative damage correlate with cognitive deficits in rats with chronic cerebral hypoperfusion. *Neurobiol Learn Mem* 2014; **109**: 7–19.
2 Cechetti F, Pagnussat AS, Worm PV, Elsner VR, Ben J, da Costa MS *et al.* Chronic brain hypoperfusion causes early glial activation and neuronal death, and subsequent long-term memory impairment. *Brain Res Bull* 2012; **87**: 109–116.
3 Okamoto Y, Yamamoto T, Kalaria RN, Senzaki H, Maki T, Hase Y *et al.* Cerebral hypoperfusion accelerates cerebral amyloid angiopathy and promotes cortical microinfarcts. *Acta Neuropathol* 2012; **123**: 381–394.
4 Rodriguez-Perez AI, Dominguez-Meijide A, Lanciego JL, Guerra MJ, Labandeira-Garcia JL. Dopaminergic degeneration is enhanced by chronic brain hypoperfusion and inhibited by angiotensin receptor blockage. *Age (Dordr)* 2013; **35**: 1675–1690.
5 Wakita H, Tomimoto H, Akiguchi I, Matsuo A, Lin JX, Ihara M *et al.* Axonal damage and demyelination in the white matter after chronic cerebral hypoperfusion in the rat. *Brain Res* 2002; **924**: 63–70.
6 Soria G, Tudela R, Marquez-Martin A, Camon L, Batalle D, Munoz-Moreno E *et al.* The ins and outs of the BCCAo model for chronic hypoperfusion: a multimodal and longitudinal MRI approach. *PLoS One* 2013; **8**: e74631.
7 Sarti C, Pantoni L, Bartolini L, Inzitari D. Cognitive impairment and chronic cerebral hypoperfusion: what can be learned from experimental models. *J Neurol Sci* 2002; **203-204**: 263–266.
8 Tsuchiya M, Sako K, Yura S, Yonemasu Y. Cerebral blood flow and histopathological changes following permanent bilateral carotid artery ligation in Wistar rats. *Exp Brain Res* 1992; **89**: 87–92.
9 Schmidt-Kastner R, Truettner J, Lin B, Zhao W, Saul I, Busto R *et al.* Transient changes of brain-derived neurotrophic factor (BDNF) mRNA expression in hippocampus during moderate ischemia induced by chronic bilateral common carotid artery occlusions in the rat. *Brain Res Mol Brain Res* 2001; **92**: 157–166.
10 Ulrich PT, Kroppenstedt S, Heimann A, Kempski O. Laser-Doppler scanning of local cerebral blood flow and reserve capacity and testing of motor and memory functions in a chronic 2-vessel occlusion model in rats. *Stroke* 1998; **29**: 2412–2420.
11 Jian H, Yi-Fang W, Qi L, Xiao-Song H, Gui-Yun Z. Cerebral blood flow and metabolic changes in hippocampal regions of a modified rat model with chronic cerebral hypoperfusion. *Acta Neurol Belg* 2013; **113**: 313–317.
12 Tomimoto H, Ihara M, Wakita H, Ohtani R, Lin JX, Akiguchi I *et al.* Chronic cerebral hypoperfusion induces white matter lesions and loss of oligodendroglia with DNA fragmentation in the rat. *Acta Neuropathol* 2003; **106**: 527–534.
13 Busch HJ, Buschmann IR, Mies G, Bode C, Hossmann KA. Arteriogenesis in hypoperfused rat brain. *J Cereb Blood Flow Metab* 2003; **23**: 621–628.
14 Chiu FY, Kao YH, Teng MM, Chung HW, Chang FC, Cho IC *et al.* Validation and absolute quantification of MR perfusion compared with CT perfusion in patients with unilateral cerebral arterial stenosis. *Eur J Radiol* 2012; **81**: 4087–4093.
15 Richardson JD, Baker JM, Morgan PS, Rorden C, Bonilha L, Fridriksson J. Cerebral perfusion in chronic stroke: implications for lesion-symptom mapping and functional MRI. *Behav Neurol* 2011; **24**: 117–122.
16 Choy M, Ganesan V, Thomas DL, Thornton JS, Proctor E, King MD *et al.* The chronic vascular and haemodynamic response after permanent bilateral common carotid occlusion in newborn and adult rats. *J Cereb Blood Flow Metab* 2006; **26**: 1066–1075.
17 Yang Q, Wang X, Cui J, Wang P, Xiong M, Jia C *et al.* Bidirectional regulation of angiogenesis and miR-18a expression by PNS in the mouse model of tumor complicated by myocardial ischemia. *BMC Complement Altern Med* 2014; **14**: 183.
18 Oldendorf WH. Trophic changes in the arteries at the base of the rat brain in response to bilateral common carotid ligation. *J Neuropathol Exp Neurol* 1989; **48**: 534–547.
19 Tahuchi Y TS, Sasahara E, Inoue H, Ohtani O. Morphological changes in capilliaries in the ischemic brain in Wistar rats. *Arch Histol Cytol* 2004; **67**: 253–261.
20 Besselmann M, Liu M, Diedenhofen M, Franke C, Hoehn M. MR angiographic investigation of transient focal cerebral ischemia in rat. *NMR Biomed* 2001; **14**: 289–296.
21 Bang OY, Saver JL, Buck BH, Alger JR, Starkman S, Ovbiagele B *et al.* Impact of collateral flow on tissue fate in acute ischaemic stroke. *J Neurol Neurosurg Psychiatry* 2008; **79**: 625–629.
22 Farkas E, Luiten PG, Bari F. Permanent, bilateral common carotid artery occlusion in the rat: a model for chronic cerebral hypoperfusion-related neurodegenerative diseases. *Brain Res Rev* 2007; **54**: 162–180.
23 Otori T, Katsumata T, Muramatsu H, Kashiwagi F, Katayama Y, Terashi A. Long-term measurement of cerebral blood flow and metabolism in a rat chronic hypoperfusion model. *Clin Exp Pharmacol Physiol* 2003; **30**: 266–272.
24 Schmidt-Kastner R, Aguirre-Chen C, Saul I, Yick L, Hamasaki D, Busto R *et al.* Astrocytes react to oligemia in the forebrain induced by chronic bilateral common carotid artery occlusion in rats. *Brain Res* 2005; **1052**: 28–39.
25 Coyle P, Panzenbeck MJ. Collateral development after carotid artery occlusion in Fischer 344 rats. *Stroke* 1990; **21**: 316–321.
26 Yang YM, Feng X, Yao ZW, Tang WJ, Liu HQ, Zhang L. Magnetic resonance angiography of carotid and cerebral arterial occlusion in rats using a clinical scanner. *J Neurosci Methods* 2008; **167**: 176–183.
27 Marti HJ, Bernaudin M, Bellail A, Schoch H, Euler M, Petit E *et al.* Hypoxia-induced vascular endothelial growth factor expression precedes neovascularization after cerebral ischemia. *Am J Pathol* 2000; **156**: 965–976.
28 Boero JA, Ascher J, Arregui A, Rovainen C, Woolsey TA. Increased brain capillaries in chronic hypoxia. *J Appl Physiol (1985)* 1999; **86**: 1211–1219.
29 Calamante F TD, Pell GS, Wiersma J, Turner R. Measuring cerebral blood flow using magnetic resonance imaging techniques. *J Cereb Blood Flow Metab* 1999; **19**: 701–735.
30 Calamante F. Arterial input function in perfusion MRI: a comprehensive review. *Prog Nucl Magn Reson Spectrosc* 2013; **74**: 1–32.
31 Giesel FL, Mehndiratta A, Essig M. High-relaxivity contrast-enhanced magnetic resonance neuroimaging: a review. *Eur Radiol* 2010; **20**: 2461–2474.
32 Goetti R, O'Gorman R, Khan N, Kellenberger CJ, Scheer I. Arterial spin labelling MRI for assessment of cerebral perfusion in children with moyamoya disease: comparison with dynamic susceptibility contrast MRI. *Neuroradiology* 2013; **55**: 639–647.
33 Dai W, Garcia D, de Bazelaire C, Alsop DC. Continuous flow-driven inversion for arterial spin labeling using pulsed radio frequency and gradient fields. *Magn Reson Med* 2008; **60**: 1488–1497.
34 Koretsky AP. Early development of arterial spin labeling to measure regional brain blood flow by MRI. *Neuroimage* 2012; **62**: 602–607.
35 Wong AM, Yan FX, Liu HL. Comparison of three-dimensional pseudo-continuous arterial spin labeling perfusion imaging with gradient-echo and spin-echo dynamic susceptibility contrast MRI. *J Magn Reson Imaging* 2014; **39**: 427–433.
36 Huang D, Wu B, Shi K, Ma L, Cai Y, Lou X. Reliability of three-dimensional pseudo-continuous arterial spin labeling MR imaging for measuring visual cortex perfusion on two 3T scanners. *PLoS One* 2013; **8**: e79471.
37 Gerriets T, Stolz E, Walberer M, Muller C, Rottger C, Kluge A *et al.* Complications and pitfalls in rat stroke models for middle cerebral artery occlusion: a comparison between the suture and the macrosphere model using magnetic resonance angiography. *Stroke* 2004; **35**: 2372–2377.